

Article

Optimized Active Control of a Smart Cantilever Beam Using Genetic Algorithm

Ali Awada ^{1,*}, Rafic Younes ² and Adrian Ilinca ¹

¹ Department of Mathematics, Computer Science and Engineering, University of Quebec at Rimouski, Rimouski, QC G5L 3A1, Canada; adrian_ilinca@uqar.ca

² Faculty of Engineering, Lebanese University, Hadath, Beirut P.O. Box 6573/14, Lebanon; raficyounes@gmail.com

* Correspondence: ali.awada@uqar.ca

Abstract: Vibration is one of the most dangerous phenomena that happens to a structure. It leads to premature fatigue and eventually failure, with potentially fatal consequences. A smart structure is an excellent solution to this problem; it adds an actuator, a sensor, and an appropriate control law to the system to reduce/eliminate the vibration. This study developed a complete analytical model for a cantilever beam with a collocated PZT sensor/actuator pair. First, we used a coupling of a collocated PZT sensor and an actuator to measure and control vibration levels based on a PID control law considering the physical constraints associated with PZT operation as the voltage level of the actuator. Next, the damping coefficient of the structure was determined by using genetic algorithms best fit to satisfy specific vibration conditions. Finally, we conducted a complete optimization for sensor/actuator position and PID parameters, using genetic algorithms. Thus, this paper gives a thorough understanding of the potential vibration control of the cantilever beam.

Keywords: vibration control; piezoelectric material; genetic algorithm; optimization; analytical model



Citation: Awada, A.; Younes, R.; Ilinca, A. Optimized Active Control of a Smart Cantilever Beam Using Genetic Algorithm. *Designs* **2022**, *6*, 36. <https://doi.org/10.3390/designs6020036>

Academic Editors: Hamid Reza Karimi and Tian Syung Lan

Received: 27 January 2022

Accepted: 7 March 2022

Published: 2 April 2022

Publisher's Note: MDPI stays neutral with regard to jurisdictional claims in published maps and institutional affiliations.



Copyright: © 2022 by the authors. Licensee MDPI, Basel, Switzerland. This article is an open access article distributed under the terms and conditions of the Creative Commons Attribution (CC BY) license (<https://creativecommons.org/licenses/by/4.0/>).

1. Introduction

Even though vibration can be helpful in some applications, and we can harvest energy from it, as shown by Jamadar et al. in Reference [1], vibration is, in most cases, harmful to structures. It can lead to high cycle fatigue failure; internal rubs, especially in rotating machines; decreased productivity; and fastener loss, which is a significant concern in high-performance machinery [2]. Crawley et al. [3] and Bailey et al. [4] introduced vibration control of structures by using a piezoelectric material in the mid-1980s. Subsequently, a lot of research addressed this subject. The concept of vibration control using Piezoelectric material transforms the structure into a smart one which usually consists of four major components: an actuator, a sensor, a controller, and the structure itself [5]. Piezoelectric material is widely used for its fast response time, low weight, relatively low cost, low power consumption, easy fabrication, design flexibility, and generation of no magnetic field while converting electrical energy to mechanical one [5–7]. Moreover, these materials can be used as actuators/sensors in several forms: surface bonded patches, embedded patches, distributed layer, cylindrical stacks, screen printed layer, etc. [6]. A crucial criterion to consider for vibration control is the choice of the control law and the placement of the actuators/sensors. In the literature, a lot of research has been conducted around the first criterion, and several control laws were studied, such as direct proportional feedback control, constant negative velocity feedback, Linear Quadratic Gaussian (LQG), Linear Quadratic Regulator (LQR), Proportional Integral Derivative (PID), sliding mode, and H_2 , as detailed in Reference [8]. Kumar et al. [9] studied the direct proportional position feedback control law, the constant gain negative velocity feedback control, and the LQR optimal control. He shows that the constant gain negative velocity feedback control is more

effective than the direct proportional position feedback control. Chandrashekhara et al. [10] reached similar conclusions.

Moreover, Kumar has shown that the LQR control offers an effective control by using lower actuator voltages than the negative velocity feedback. Qui et al. [11] showed that a combined position feedback control (PPF) with a proportional derivative (PD) control can be effective in vibration suppression, especially for small-vibration amplitude. Yang et al. [7] showed the effectiveness of the velocity feedback control in vibration suppression of a composite laminated plate with different fiber orientations, using an embedded PZT actuator/sensor.

In addition, He et al. [12] proved the effectiveness of the constant velocity feedback control law in attenuating the vibration amplitude of functionally graded material (FGM) plates. Waghulde et al. [5] showed that the LQG control law can reduce 30% of a smart cantilever beam's first mode vibration response. LQR is widely used [13–16] because of its capability to stabilize the closed-loop system and allow the user to define weights on inputs and states [13]. Zhao et al. [14] tested a hybrid control consisting of a passive shunt circuit with an LQR controller and has shown better vibration attenuation. Lee et al. [17] applied the LQR controller to a system of laminated composite stiffener with PZT layers at the top and bottom. They searched the optimal position of the stiffener. Abdelrahman et al. [16] studied the effect of the size and material of PZT on vibration control. Using an LQR controller gave considerable vibration reduction in settling time and the actuation force. PID controller has also been widely used, and its effectiveness in vibration reduction has been proven [11,18,19]. Khot et al. [20] used the PID controller based on output feedback to compare the full and reduced model of a beam, and a good agreement was shown.

On the other hand, Qui et al. [21] proposed a sliding mode controller based on acceleration sensor control strategy. They have shown that this controller, along with proportional feedback control, can effectively reduce the first and second bending modes of vibration. Furthermore, Rodriguez et al. [22] confirmed the effectiveness and robustness of sliding control law to uncertainties and noise. Finally, Caruso et al. [23] proposed using multiple pairs of actuators/sensors along with an appropriate H_2 control strategy designed on a model with three vibration modes. The controller has shown high performance in vibration reduction of the clamped plate taken into consideration.

The other criterion mentioned above, the placement of the actuator/sensor, has been widely studied in the literature. Actuators should be placed in appropriate locations to excite the desired modes to control effectively [3], as performed in a study by Botta et al. [24] wherein the positions of the actuators were optimized to control each of the first five modes of vibration and combined modes of vibration. A bad positioning for the actuator and sensors leads to non-effective vibration control, and in some cases, more excitation of the spillover effect. The spillover effect comes from the fact that only the first few low-frequency modes are considered when modeling a system for vibration, and the high-frequency modes (residual modes) are treated as uncertainties. In this case, the state feedback based on the reduced model may destabilize the residual modes, as many controlled structures are lightly damped [25]. Gupta et al. [6] presented five criteria for the optimal placement of piezoelectric sensors and actuators: maximizing modal forces/moments applied to the structure by the PZT actuators, maximizing the deflection of the structure, minimizing the control energy utilized by the actuators, maximizing the degree of controllability, maximizing the degree of observability, and minimizing the effects of spillover.

Several papers have studied the optimal placement of the actuator/sensor. For example, Qui et al. [11] used an H_2 norm to maximize the plate's controllability and observability. As a result, the actuator/sensor pair's best placement for suppressing the bending modal vibration turns out to be the root of the plate; instead, for suppressing torsional vibration, the pair should be placed at the tip of the plate. The genetic algorithm was also used to study the optimal placement in References [15,26,27]. The main objective was to maximize controllability and observability and reduce the spillover effect.

In the subsequent sections, we use a couple of collocated PZT sensor and actuator to measure and control vibration levels of the damped beam based on a PID control law. In this model, we consider the physical constraints associated with PZT operation as the voltage level of the actuator. Next, the damping coefficient of the structure is determined by using genetic algorithms best fit to satisfy specific vibration conditions. Finally, we conducted a complete optimization for sensor/actuator position and PID parameters, using genetic algorithms.

The novelty of this paper resides in a thorough analysis of the beam’s vibration control and the insertion of the actuator’s physical constraints in the derivation of motion’s analytical equation, which is very important to achieve a more realistic system representation. In addition, it can improve the vibration control of the structure, since it allows us to take better advantage of the actuator by applying the best voltage without damaging it. Moreover, the use of the genetic algorithm helps optimize the vibration control by determining the actuator’s best position and the PID controller parameters.

2. Analytical Model for Damped Cantilevered Beam Controlled with PZT Actuator

Obtaining a dynamic system model is very important during structural vibration control systems analysis. There are three standard techniques for procuring models of flexible structures [28]: The first is the finite element analysis, which is an approximate method giving a high-order spatially discrete system. This method was widely used in the literature to obtain a model for a cantilevered structure with a PZT actuator/sensor. The second technique is system identification, which uses experimental data to identify composite structural and piezoelectric model parameters. The third one is the analytical model, which uses the modal approach to obtain and solve the partial differential equation of the system.

Figure 1 shows a schematic of the controlled damped cantilever beam used to build the analytical model. As shown in Figure 1, we have a beam with a pair of PZT patches fixed in position x_1 . One acts as an actuator at the beam’s top, and the second, fixed at the bottom, acts as a sensor. Moreover, an initial load, P , is applied to the tip of the beam.

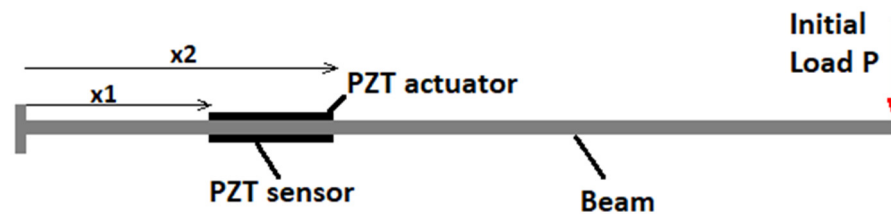


Figure 1. Schematic of the cantilevered beam with PZT actuator/sensor pair.

In this study, we did not consider the beam’s mass-induced deformation. The partial differential equation describing the system of a cantilever beam with the pair of sensor/actuator is as follows [28]:

$$E_b I_b \frac{\partial^4 \omega(x, t)}{\partial x^4} + \rho_b A_b \frac{\partial^2 \omega(x, t)}{\partial t^2} + c_b \frac{\partial \omega(x, t)}{\partial t} = M_a \left(\frac{\partial \delta}{\partial x(x-x_2)} - \frac{\partial \delta}{\partial x(x-x_1)} \right) \quad (1)$$

where M_a is the moment applied by the PZT actuator, δ is the Dirac function, c_b is the damping coefficient of the beam, and x_1 and x_2 are the coordinates of the PZT actuator.

Appendix A explains, in detail, the different terms of the partial differential equation of the system (1).

The moment applied by the PZT actuator can be defined as follows [13]:

$$M_a = -E_a \cdot b_a \cdot d_{31} \cdot \left(\frac{h_b + h_a}{2} \right) \cdot \frac{I_b}{I_{eq}} V_a = K^* \cdot \frac{I_b}{I_{eq}} \cdot V_a = K_a \cdot V_a \quad (2)$$

where E_a , b_a , d_{31} , h_b , h_a , V_a , I_b , and I_{eq} represent, respectively, Young’s modulus of the PZT actuator, the width of the actuator, the piezoelectric strain constant, beam height, PZT actuator height, applied actuator voltage, the moment of inertia of the beam, and the equivalent moment of inertia of the beam with the PZT pair of actuator/sensor.

In this study, since the pair of actuator/sensor has the exact dimensions; thus, $h_a = h_s$ and $b_a = b_s$, where h_s and b_s are the height and the width of the sensor.

I_{eq} can be defined as follows [13]:

$$I_{eq} = \frac{b_b h_b^3}{12} + \frac{b_a eq h_a^3}{12} + b_a h_a \left(\frac{h_b}{2} + \frac{h_a}{2} \right)^2 + \frac{b_s eq h_s^3}{12} + b_s h_s \left(\frac{h_b}{2} + \frac{h_s}{2} \right)^2$$

$$I_{eq} = \frac{b_b h_b^3}{12} + 2 \frac{b_a eq h_a^3}{12} + 2 b_a h_a \left(\frac{h_b}{2} + \frac{h_a}{2} \right)^2$$

and $b_a eq = b_s eq = b_a \cdot \frac{E_a}{E_b}$ is the equivalent PZT width.

As we can see in Equation (1), the choice of the control law will affect all the subsequent model calculations. This study used a Proportional Integral Derivative (PID) controller based on the sensor voltage. The system’s movement dictates the sensor voltage signal. This controller aims to reduce the system vibration, reaching stable sensor voltage. In this case, the voltage fed to the actuator becomes the following:

$$V_a = K_P \cdot (V_s - V_{desired}) + K_D \cdot (\dot{V}_s - \dot{V}_{desired}) + K_I \cdot \int (V_s - V_{desired}) dt \tag{3}$$

where K_P , K_D , and K_I are the parameters of the controller, and $V_{desired}$ represents the desired sensor voltage. In our case, the desired sensor voltage is zero, as we try to reduce and eventually stop the system’s vibration. V_s is the measured sensor voltage:

$$V_s = -E_s \cdot b_s \cdot \frac{g_{31}}{2C} \left(\frac{h_b}{2} \right) \cdot \left. \frac{\partial \omega(x, t)}{\partial x} \right|_{x_1}^{x_2} = K_s \cdot \left. \frac{\partial \omega(x, t)}{\partial x} \right|_{x_1}^{x_2}$$

where E_s , b_s , g_{31} , and C represent, respectively, Young’s modulus of the PZT sensor, the width of the sensor, the piezoelectric voltage coefficient, and the capacitance of the PZT sensor.

Thus, we have the following:

$$V_a = K_P \cdot V_s + K_D \cdot \dot{V}_s + K_I \cdot \int V_s dt \tag{4}$$

Figure 2 shows the schematic of the PID controller. The PID controller uses the sensor voltage to calculate the appropriate voltage applied to the actuator.

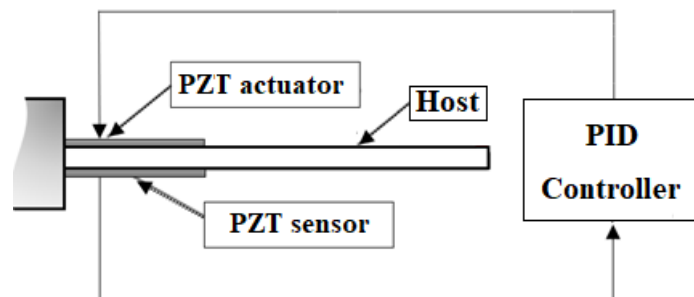


Figure 2. Schematic of the controller.

By substituting all the variables mentioned above in Equation (1), we obtain the general equation:

$$\begin{aligned}
 E_b I_b \frac{\partial^4 \omega(x,t)}{\partial x^4} &+ \rho_b A_b \frac{\partial^2 \omega(x,t)}{\partial t^2} + c_b \frac{\partial \omega(x,t)}{\partial t} \\
 &= K_a \cdot K_s \cdot \left(K_P \cdot \frac{\partial \omega(x,t)}{\partial x} \Big|_{x_1}^{x_2} + K_I \cdot \int \frac{\partial \omega(x,t)}{\partial x} \Big|_{x_1}^{x_2} dt \right. \\
 &\quad \left. + K_D \cdot \frac{\partial}{\partial t} \frac{\partial \omega(x,t)}{\partial x} \Big|_{x_1}^{x_2} \right) \cdot \left(\frac{\partial \delta}{\partial x(x-x_2)} - \frac{\partial \delta}{\partial x(x-x_1)} \right)
 \end{aligned} \tag{5}$$

The displacement $\omega(x,t)$ can be separated in space and time by using the modal analysis approach [29]:

$$\omega(x,t) = \sum_{i=1}^{\infty} \phi_i(x) f_i(t) \tag{6}$$

Here, $\phi_i(x)$ represents the eigenfunction and is known as the mode-shape. In our case, we assume that the actuator’s impacts on mode shapes are insignificant, which is true if the actuator’s dimensions are tiny compared to the beam’s [13]. Thus, the mode-shape equation for a cantilevered beam is as follows [30,31]:

$$\phi_i(x) = \frac{1}{2} \left[\cos(\gamma_i L) - \cos h(\gamma_i L) + \left(\frac{-\cos(\gamma_i L) - \cos h(\gamma_i L)}{\sin(\gamma_i L) + \sin h(\gamma_i L)} \right) (\sin(\gamma_i L) - \sin h(\gamma_i L)) \right] \tag{7}$$

where $\gamma_i^4 = \frac{\omega_i^2}{c^2}$.

Moreover, $c = \sqrt{\frac{E_b I_b}{\rho_b A_b}}$. Substituting Equation (6) in (5), multiplying by $\phi_j(x)$, and integrating over all the length of the beam gives the following:

$$\begin{aligned}
 \sum_{i=1}^n \int_0^L \left(E_b I_b \cdot f_i(t) \phi_j(x) \cdot \frac{\partial^4 \phi_i(x)}{\partial x^4} + \rho_b A_b \cdot \phi_j(x) \cdot \phi_i(x) \frac{\partial^2 f_i(t)}{\partial t^2} \right. \\
 \left. + c_b \cdot \phi_j(x) \cdot \phi_i(x) \frac{\partial f_i(t)}{\partial t} \right) dx \\
 = \int_0^L \left\{ K_a \cdot K_s \sum_{i=1}^n \left(K_P \cdot f_i(t) \cdot \phi_j(x) \frac{\partial \phi_i(x)}{\partial x} \Big|_{x_1}^{x_2} \right. \right. \\
 = K_I \cdot \phi_j(x) \frac{\partial \phi_i(x)}{\partial x} \Big|_{x_1}^{x_2} \cdot \int f_i(t) dt \\
 \left. \left. + K_D \cdot \frac{\partial f_i(t)}{\partial t} \cdot \phi_j(x) \frac{\partial \phi_i(x)}{\partial x} \Big|_{x_1}^{x_2} \right) \cdot \left(\frac{\partial \delta}{\partial x(x-x_2)} - \frac{\partial \delta}{\partial x(x-x_1)} \right) \right\} dx
 \end{aligned} \tag{8}$$

Using the property of orthogonality of the mode-shapes results in the following [29]:

$$\int_0^L \phi_j(x) \phi_i(x) dx = \delta_{ij}$$

where $\delta_{ij} = \begin{cases} 1 & \text{if } i = j \\ 0 & \text{otherwise} \end{cases}$

In addition, using the property of the Dirac Delta function, we achieve the following:

$$\int_{-\infty}^{\infty} \delta^{(n)}(x - \theta) \phi(x) dx = (-1)^n \phi^{(n)}(\theta)$$

The Equation (8) can be reduced to the following:

$$\begin{aligned}
 E_b I_b \cdot f_i(t) \int_0^L \phi_i(x) \cdot \frac{\partial^4 \phi_i(x)}{\partial x^4} dx + \rho_b A_b \cdot \frac{\partial^2 f_i(t)}{\partial t^2} + c_b \cdot \frac{\partial f_i(t)}{\partial t} \\
 = K_a \cdot K_s \cdot \left(\frac{\partial \phi_i(x)}{\partial x} \Big|_{x_1}^{x_2} \right) \cdot [K_P \cdot f_i(t) + K_I \cdot \int f_i(t) dt \\
 + K_D \cdot \frac{\partial f_i(t)}{\partial t}]
 \end{aligned} \tag{9}$$

Regrouping terms give the following:

$$\ddot{f}_i(t) + \frac{c_b}{\rho_b A_b} \dot{f}_i(t) + \Omega^2 f_i(t) = K_{Ti} \cdot \left(K_P \cdot f_i(t) + K_D \dot{f}_i(t) + K_I \int f_i(t) dt \right) \tag{10}$$

where $\Omega^2 = \frac{E_b I_b}{\rho_b A_b} \int_0^L \phi_i(x) \cdot \frac{\partial^4 \phi_i(x)}{\partial x^4} dx$

$$K_{Ti} = K_a \cdot K_s \cdot \left(\frac{\partial \phi_i(x)}{\partial x} \Big|_{x_1}^{x_2} \right)^2$$

To solve Equation (10), the integral term of the PID was integrated by iterations of solving the following equation:

$$\begin{aligned} \ddot{f}_i(t) + \frac{c_b}{\rho_b A_b} \dot{f}_i(t) + \Omega^2 f_i(t) &= K_{Ti} \cdot (K_P \cdot f_i(t) + K_D \dot{f}_i(t) \\ &+ K_I (f_i(t) + f_i(t-1) + \dots + f_i(0))) \end{aligned} \tag{11}$$

At time, t , all the precedent $f_i(t-1), f_i(t-2), \dots, f_i(0)$ are already calculated and can be inserted as coefficients, a_i .

Thus Equation (11) can be organized as follows:

$$\ddot{f}_i(t) + \left(\frac{c_b}{\rho_b A_b} + K_i \cdot K_D \right) \dot{f}_i(t) + \left(\Omega^2 + K_{Ti} K_P + K_{Ti} \cdot K_I \right) f_i(t) + a_i = 0 \tag{12}$$

Equation (12) is for the i th vibration mode. If we truncate to the first n vibration modes, the dynamics of the system can be represented by the state-space equation:

$$\dot{Z}(t) - D \cdot Z(t) = A \tag{13}$$

where $Z(t) = \left[f_1(t), f_2(t), \dots, f_n(t), \dot{f}_1(t), \dot{f}_2(t), \dots, \dot{f}_n(t) \right]^T$ represents the state vector.

In this study, we chose n equal three, considering that the first three modes have the greatest impact on the vibration response.

The other terms in Equation (13) are as follows:

$$D = \begin{bmatrix} 0_{n \times n} & I_{n \times n} \\ \Omega^2 + K_{Ti} K_P + K_{Ti} \cdot K_I & \frac{c_b}{\rho_b A_b} + K_i \cdot K_D \end{bmatrix}$$

$$A = \begin{bmatrix} 0_{n \times 1} \\ a_1 \\ a_2 \\ \vdots \\ a_n \end{bmatrix}$$

At this level, we here introduce the voltage limit of the PZT actuator. A PZT actuator can hold $|V_a| \leq V_{limit}$. Otherwise, the actuator will crack as the generated tensile stress in PZT exceeds the fracture tensile strength of the material [32].

The methodology used in our code to solve this system is to check at every iteration of time, t , the actuator voltage, and if this voltage is higher than the limit voltage, the voltage attributed to the actuator becomes $\pm V_{limit}$ based on the sign of V_a . Equation (5) then becomes as follows:

$$\begin{aligned} E_b I_b \frac{\partial^4 \omega(x,t)}{\partial x^4} + \rho_b A_b \frac{\partial^2 \omega(x,t)}{\partial t^2} + c_b \frac{\partial \omega(x,t)}{\partial t} &= K_a \cdot \pm V_{limit} \cdot \left(\frac{\partial \delta}{\partial x}(x-x_2) - \frac{\partial \delta}{\partial x}(x-x_1) \right) \end{aligned} \tag{14}$$

After performing all of the above mentioned subsequent steps, the final equation to solve is as follows:

$$\ddot{f}_i(t) + \frac{c_b}{\rho_b A_b} \dot{f}_i(t) + \Omega^2 f_i(t) = K_a \cdot \pm V_{limit} \cdot \left. \frac{\partial \phi_i(x)}{\partial x} \right|_{x_1}^{x_2} \tag{15}$$

As we can see, the right-handed side of the equation is time-independent, and it can be replaced by a coefficient, a_i^* , and the state-space equation is as follows:

$$\dot{Z}(t) - D^* \cdot Z(t) = A^* \tag{16}$$

where

$$D^* = \begin{bmatrix} 0_{n \times n} & I_{n \times n} \\ \Omega^2 & \frac{c_b}{\rho_b A_b} \end{bmatrix}$$

$$A^* = \begin{bmatrix} 0_{n \times 1} \\ a_1^* \\ a_2^* \\ \vdots \\ a_n^* \end{bmatrix}$$

Figure 3 shows the methodology used in our MATLAB code to solve the equation of motion of the beam controlled by the PZT actuator, with a PID voltage controller and considering the voltage limit that the actuator can withstand. After calculating $Z(t)$ in Equations (13) and (16), as in Figure 3, the final solution of $\omega(x, t)$ can be calculated by using Equation (6).

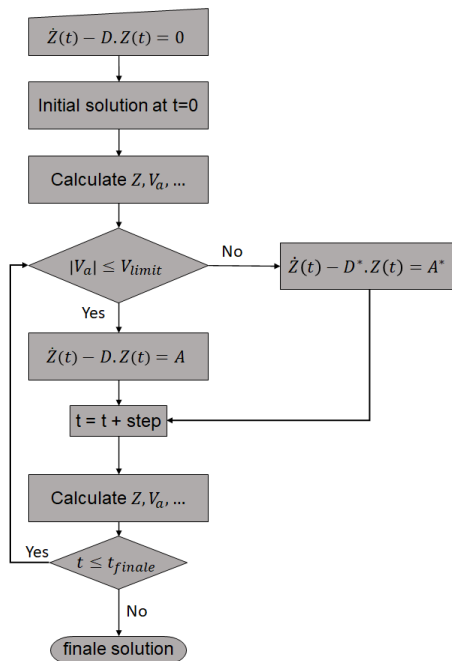


Figure 3. Methodology of solving the equation, considering the voltage limit of the actuator.

3. Optimization Using Genetic Algorithm

The genetic algorithm (GA) is one of the earliest population-based stochastic algorithms proposed in history [33]. This research method that was developed by John Holland back in 1975 [34] is inspired by natural Darwinian evolution [35]. In GA, every individual is a candidate (chromosome) whose fitness is evaluated every iteration, using an objective function known as the fitness function. Best individuals are chosen randomly by using a

selection mechanism, and these candidates are used to improve other solutions, using the crossover between individuals. The crossover consists of exchanging genetic material of two parents at a random position in the chromosomes to produce a new child exploiting the area between the parents, as shown in Figure 4. The parents' chromosomes, blue and red, are exchanged at a specific position (single point or double point, as shown in the figure) to obtain children with alternating blue and red chromosomes. GA also randomly adds new genetic information to the so-called "mutation" search process. This process adds diversity to the population and helps avoid local optimal solutions [35]. Figure 5 shows an example of how the mutation method processes. The genetic information of the randomly chosen chromosomes for the children is changed from zero to one, as shown in the figure.

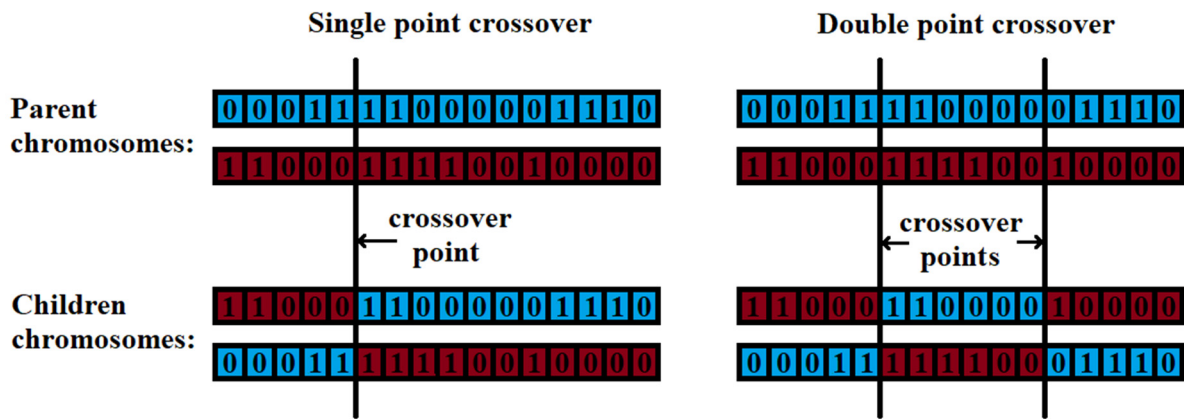


Figure 4. Single-point and double-point crossover.

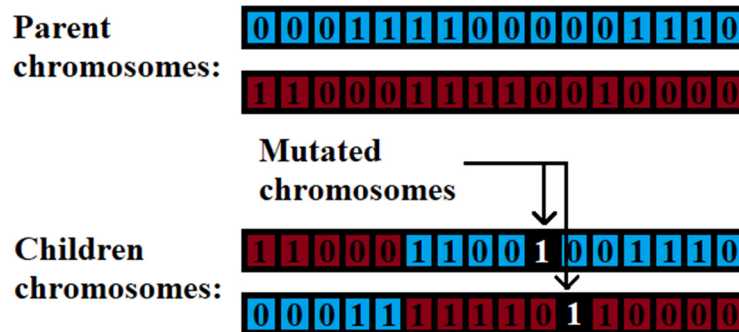


Figure 5. Example of the mutation process.

It must be noted that the evaluation process is based on the fitness function; p_c is the parameter representing the probability of crossover, usually between 0.5 and 1; and p_m is the probability of mutation, and it is usually very low, i.e., less than 0.05 [36].

We first used GA as a search technique to determine the structural damping coefficient of the beam with a prescribed vibration attenuation. After that, we used it to optimize the pair of PZT sensor/actuator placement. Finally, we used it to determine the optimal PID parameters.

3.1. Finding the Damping Coefficient of the Structure

The damping coefficient is very difficult to determine in any structure. In our case, we assume that the structural damping coefficient is such that the tip displacement is reduced by 60% after 10 s. Therefore, we need to find the appropriate damping coefficient that helps reach this attenuation. We used the genetic algorithm to determine the value that respects the desired conditions. Here, the objective was to determine the damping coefficient " c_b " that gives an attenuation of 60% of the tip displacement after $t_{finale} = 10$ s of free vibration. The fitness function chosen minimizes the error between data " $\omega_s(L, t)$ " from

the searched c_b , using the GA and the desired tip displacement “ $\omega_d(L, t)$ ” (free undamped tip displacement with 60% attenuation after 10 s). The fitness function is defined as follows:

$$J = \int_0^{t_{finale}} [\omega_s(L, t) - \omega_d(L, t)]^2 dt$$

The parameter of the aluminum beam used and the PZT-5H actuator/sensor are summarized in Table 1.

Table 1. Summary of characteristics of the beam and PZT actuator/sensor pair.

Parameter	Value
Length of the beam L (m)	1
Width of the beam w_b (m)	0.3
Thickness of the beam h_b (m)	0.004
Beam Young’s modulus E_b (Pa)	69×10^9
Density of the beam ρ_b (kg/m ³)	2705
Damping coefficient c	0.5079
Initial load applied to beam’s tip P (N)	7.038
Length of PZT L_p (m)	0.1
Width of PZT w_p (m)	0.1
Thickness of PZT h_p (m)	0.002
PZT Young’s modulus E_p (Pa)	6.4×10^{10}
Density of PZT ρ_p (kg/m ³)	7500
Piezoelectric constant d_{31} (C/N)	-274×10^{-12}
Piezoelectric voltage coefficient g_{31} (V/N)	-0.15099
Free dielectric constant K_3^T	3400
PZT capacitance C_p [37]	0.3008

The obtained “ c_b ” was 0.5079. Figure 6 shows a good agreement between the tip displacement of the beam, with “ c_b ” obtained by using the GA and the desired tip displacement.

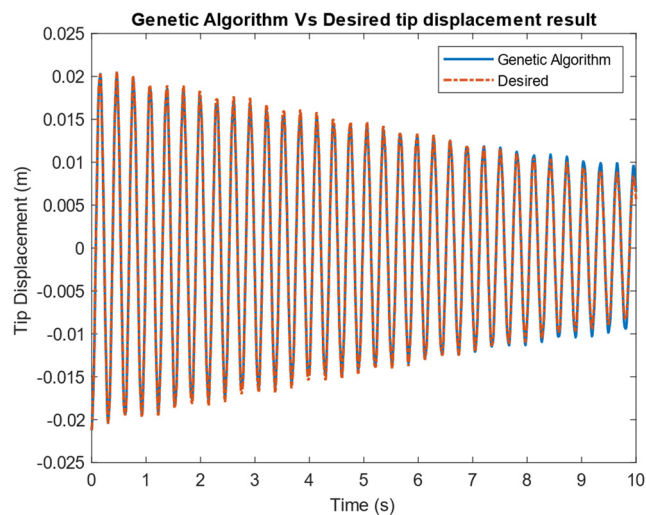


Figure 6. Comparison of tip displacement for the obtained ‘ c_b ’ from GA and the desired attenuation.

3.2. Optimization of the Actuator Position

As mentioned above, the actuator position has a crucial role in controlling the structure. In our case, GA was used to obtain the actuator’s best position to attenuate the vibration of the beam’s tip. This study aimed to reduce the tip displacement as much as possible

with the control of the first three vibration modes, as mentioned above. Thus, the fitness function (objective function) is used to minimize the tip displacement:

$$J = \int_0^{t_{final}} [\omega_s(L, t) - \omega_d(L, t)]^2 dt$$

where $t_{final} = 10$ s, $\omega_s(L, t)$ is the tip displacement based on parameters defined in the GA optimization process and $\omega_d(L, t)$ is the desired tip displacement (equal to zero).

Using the GA, the optimal x_1 found was zero near the fixed end of the beam. To test this result, the controller parameters (K_P , K_D , and K_I) were fixed as follows:

$$\begin{aligned} K_P &= -1,000,000 \\ K_I &= 0 \\ K_D &= -1,000,000 \end{aligned}$$

and several positions of the actuator were tested. As shown in Figure 7, a good agreement with the GA results is obtained. The actuator becomes less and less efficient when moving away from the fixed end. The controller itself introduces an instability (vibration increase) for $x_1 = 0.3$.

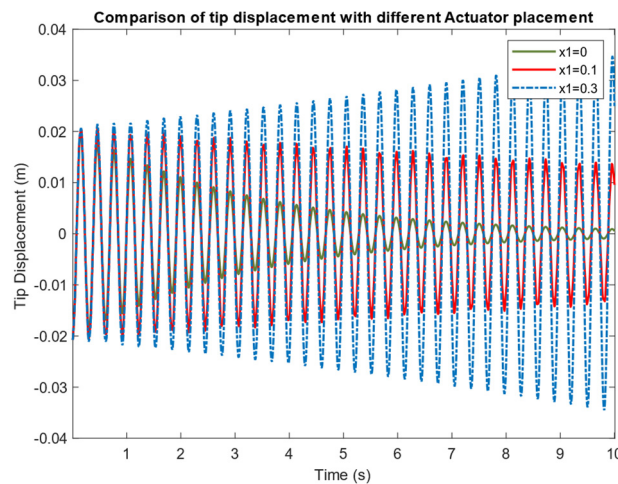


Figure 7. Comparison of tip displacement with different actuator placement.

3.3. Optimization of Controller Parameter Using GA

Considering the complexity to determine the optimal parameters of the PID controller explained above, the genetic algorithm was used to find the best values of K_P , K_D , and K_I . The objective function is again to minimize the beam’s tip displacement:

$$J = \int_0^{t_{final}} [\omega_s(L, t) - \omega_d(L, t)]^2 dt$$

where $t_{final} = 10$ s, $\omega_s(L, t)$ is the tip displacement based on parameters defined in the GA optimization process and $\omega_d(L, t)$ is the desired tip displacement (equal to zero). The beam’s damping coefficient is ‘ $c = 0.5079$ ’, as obtained above (Section 3.1), and the position of the actuator/sensor pair is given by the previous optimization (Section 3.2), ‘ $x_1 = 0$ ’. V_{limit} is 150 V.

The best PID parameters obtained by using the GA were as follows:

$$K_P = -500,227,077.54$$

$$K_I = 0.329$$

$$K_D = -69,151,875.29$$

As shown in Figure 8, the PID controller with optimized parameters using the GA helps eliminate the structure’s vibration in less than 0.4 s. Without control, the beam takes over 20 s until vibration stops.

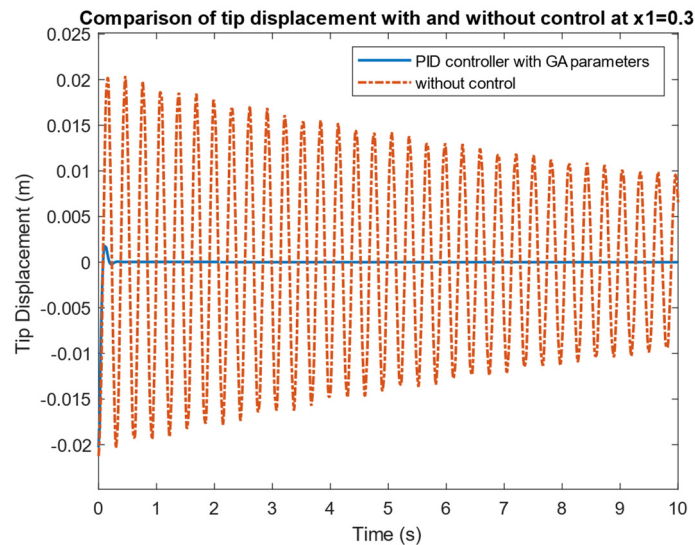


Figure 8. Tip displacement of the beam with PID controller with optimized parameters using GA and without control.

As shown in Figure 9, the voltage limit of 150 V helps reach the stability of the structure more rapidly, as it exploits the capacity of the actuator more efficiently.

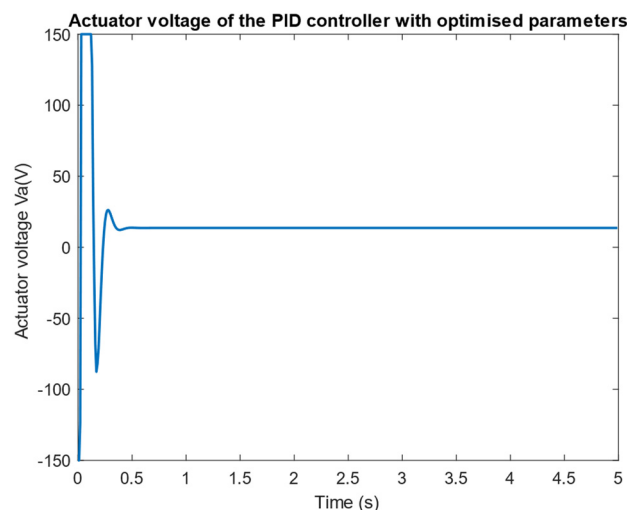


Figure 9. Actuator voltage of the PID controller with optimized parameters.

To better understand the integration of voltage limit in the model, a test compares the model with voltage limit with a model without voltage limit. In fact, in the case of the model without a voltage limit, one can never know precisely the voltage of the actuator, and it can mount to unrealistic values. We took a case when the PID controller parameters give an actuator voltage near 150 V without exceeding it. Figure 10 shows that, in this case,

the beam needs a lot more time to stabilize than the model with a voltage limit. Figure 11 shows the exploitation of the two models for the actuator voltage. As we can see, the model with a voltage limit gives a more stable response and fast vibration suppression.

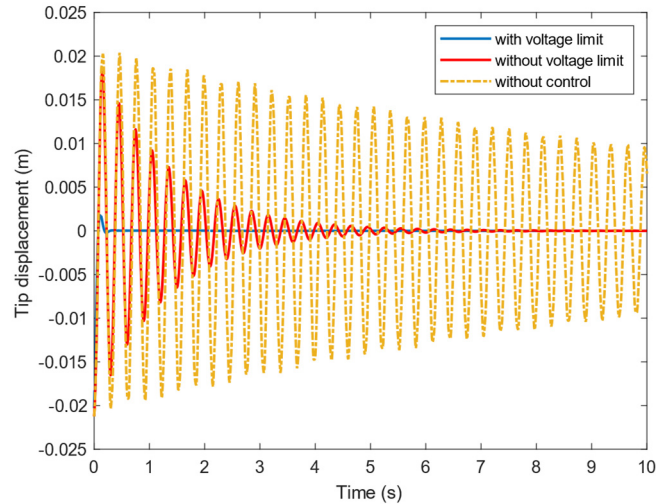


Figure 10. Comparison between beam response with voltage limit, without voltage limit, and without control.

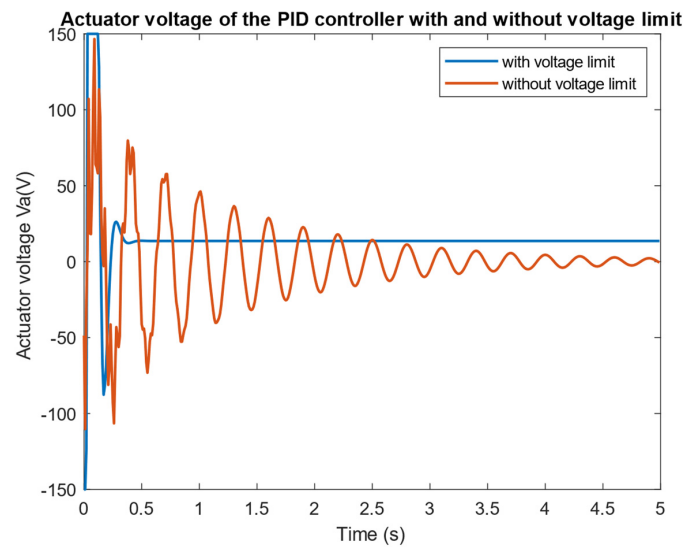


Figure 11. Actuator voltage of the PID controller with and without voltage limit.

4. Conclusions

This paper presented the analytical vibration models of a damped cantilevered beam controlled with a PID controller. The model considered the damping coefficient of the beam and the integration of the voltage limit for the PZT actuator. This model can be used to add multiple actuators. This paper presents the step-by-step method of resolution of this model. Furthermore, the genetic algorithm was used to find the damping coefficient, optimize the PZT actuator position, and determine the optimal parameters of the PID controller. Analytical results show a good efficiency of the PID controller in suppressing the vibration.

Moreover, integrating the actuator voltage limit leads to fast vibration elimination. This method is different from traditional control. It helps the controller take advantage of the capacity of the actuators without damaging its physical structure and eventually avoid its premature fatigue and failure. The results in this paper can be used in oncoming research to validate experimental or numerical methods subsequently applied for more complex geometries for which analytical models are not available.

The proposed system has multiple applications. It can control the wind turbine blade vibration by adding an appropriate number of PZT actuators. In aviation, the PZT system is particularly advantageous, as the lightweight of the vibration control system is crucial. It can be used in most applications having vibration problems. For example, we have implemented this system to control an approximate model of a wind turbine blade. The results are encouraging and will be submitted soon for publication.

Author Contributions: Conceptualization, A.A.; methodology, A.A.; software, A.A.; validation, A.A.; formal analysis, A.A.; investigation, A.A.; resources, A.A.; data curation, A.A.; writing—original draft preparation, A.A.; writing—review and editing, A.A., A.I. and R.Y.; supervision, R.Y. and A.I.; project administration, A.I. and R.Y.; funding acquisition, A.I. All authors have read and agreed to the published version of the manuscript.

Funding: The authors acknowledge the financial support from NSERC Canada (Natural Sciences and Engineering Research Council) through a Discovery Grant.

Institutional Review Board Statement: Not applicable.

Informed Consent Statement: Not applicable.

Data Availability Statement: Not applicable.

Acknowledgments: I would like to thank my parents and my wife. Without their tremendous understanding and encouragement in the past few years, it would have been impossible to continue my research.

Conflicts of Interest: The authors declare no conflict of interest.

Appendix A

As the force applied by the PZT actuator can be represented at its ends, x_1 and x_2 , the partial differential equation describing the system of the cantilever beam with a PZT actuator can be written in the following form:

$$E_b I_b \frac{\partial^4 \omega(x,t)}{\partial x^4} + \rho_b A_b \frac{\partial^2 \omega(x,t)}{\partial t^2} + c_b \frac{\partial \omega(x,t)}{\partial t} = F_{x_2} - F_{x_1}$$

$$E_b I_b \frac{\partial^4 \omega(x,t)}{\partial x^4} + \rho_b A_b \frac{\partial^2 \omega(x,t)}{\partial t^2} + c_b \frac{\partial \omega(x,t)}{\partial t} = F \cdot (\delta_{(x-x_2)} - \delta_{(x-x_1)})$$

where F_{x_2} and F_{x_1} are the forces applied by the PZT actuator on the beam.

Point Moment:

If we consider a force, F , with a distance of d , as represented in Figure A1, then the resultant moment is $M = F \cdot d$.

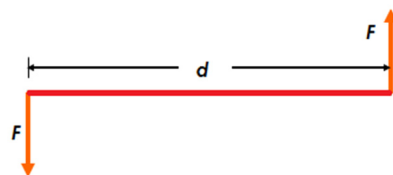


Figure A1. Schematic of forces applied to a beam.

When $d \rightarrow 0$,
then

$$F_x = \lim_{d \rightarrow 0} (F \delta_x - F \delta_{x-d})$$

$$= \lim_{d \rightarrow 0} \left(\frac{M}{d} \delta_x - \frac{M}{d} \delta_{x-d} \right)$$

$$= M \lim_{d \rightarrow 0} \left(\frac{\delta_x - \delta_{x-d}}{d} \right)$$

$$F_x = M \cdot \frac{\partial \delta}{\partial x_x}$$

Based on this, $F \cdot (\delta_{(x-x_2)} - \delta_{(x-x_1)})$ mentioned above can be written in the following form:

$$M_a \left(\frac{\partial \delta}{\partial x (x-x_2)} - \frac{\partial \delta}{\partial x (x-x_1)} \right)$$

References

- Jamadar, V.M.; Rade, K.A.; Kanase, S.S.; Suryawanshi, A.S. Vibration Energy Harvesting From Power Producing Devices. *Int. J. Adv. Mech. Eng.* **2018**, *8*, 153–159.
- Palazzolo, A. *Vibration Theory and Applications with Finite Elements and Active Vibration Control*; John Wiley & Sons: Hoboken, NJ, USA, 2016.
- Crawley, E.F.; De Luis, J. Use of piezoelectric actuators as elements of intelligent structures. *AIAA J.* **1987**, *25*, 1373–1385. [[CrossRef](#)]
- Bailey, T.; Hubbard, J.E., Jr. Distributed piezoelectric-polymer active vibration control of a cantilever beam. *J. Guid. Control Dyn.* **1985**, *8*, 605–611. [[CrossRef](#)]
- Waghulde, K.; Sinha, B.; Patil, M.; Mishra, S. Vibration Control of Cantilever Smart Beam by using Piezoelectric Actuators and Sensors. *Int. J. Eng. Technol.* **2010**, *2*, 259–262.
- Gupta, V.; Sharma, M.; Thakur, N. Optimization criteria for optimal placement of piezoelectric sensors and actuators on a smart structure: A technical review. *J. Intell. Mater. Syst. Struct.* **2010**, *21*, 1227–1243. [[CrossRef](#)]
- Yang, S.; Bian, J. Vibration suppression experiments on composite laminated plates using an embedded piezoelectric sensor and actuator. *Smart Mater. Struct.* **1996**, *5*, 501. [[CrossRef](#)]
- Awada, A.; Younes, R.; Ilinca, A. Review of Vibration Control Methods for Wind Turbines. *Energies* **2021**, *14*, 3058. [[CrossRef](#)]
- Kumar, K.R.; Narayanan, S. Active vibration control of beams with optimal placement of piezoelectric sensor/actuator pairs. *Smart Mater. Struct.* **2008**, *17*, 055008. [[CrossRef](#)]
- Chandrashekhara, K.; Agarwal, A. Active vibration control of laminated composite plates using piezoelectric devices: A finite element approach. *J. Intell. Mater. Syst. Struct.* **1993**, *4*, 496–508. [[CrossRef](#)]
- Qiu, Z.; Zhang, X.; Wu, H.; Zhang, H. Optimal placement and active vibration control for piezoelectric smart flexible cantilever plate. *J. Sound Vib.* **2007**, *301*, 521–543. [[CrossRef](#)]
- He, X.; Ng, T.; Sivashanker, S.; Liew, K. Active control of FGM plates with integrated piezoelectric sensors and actuators. *Int. J. Solids Struct.* **2001**, *38*, 1641–1655. [[CrossRef](#)]
- Devasia, S.; Meressi, T.; Paden, B.; Bayo, E. Piezoelectric actuator design for vibration suppression-placement and sizing. *J. Guid. Control Dyn.* **1993**, *16*, 859–864. [[CrossRef](#)]
- Zhao, Y. Vibration suppression of a quadrilateral plate using hybrid piezoelectric circuits. *J. Vib. Control* **2010**, *16*, 701–720. [[CrossRef](#)]
- Bruant, I.; Gallimard, L.; Nikoukar, S. Optimal piezoelectric actuator and sensor location for active vibration control, using genetic algorithm. *J. Sound Vib.* **2010**, *329*, 1615–1635. [[CrossRef](#)]
- Abdelrahman, W.G.; Al-Garni, A.Z.; Abdelmaksoud, S.I.; Abdallah, A. Effect of Piezoelectric Patch Size and Material on Active Vibration Control of Wind Turbine Blades. *J. Vib. Eng. Technol.* **2018**, *6*, 155–161. [[CrossRef](#)]
- Lee, C.-Y.; Jung, J.-Y.; Jeong, S.-M. Active vibration suppression of stiffened composite panels with piezoelectric materials under blast loads. *Appl. Sci.* **2020**, *10*, 387. [[CrossRef](#)]
- Kumar, S.; Srivastava, R.; Srivastava, R. Active vibration control of smart piezo cantilever beam using pid controller. *Int. J. Res. Eng. Technol.* **2014**, *3*, 392–399.
- Labanie, M.F.; Ali, J.M.; Dawood, M.S. Optimal location of piezoelectric patches for active vibration control. *IOP Conf. Ser.: Mater. Sci. Eng.* **2017**, *184*, 012012. [[CrossRef](#)]
- Khot, S.; Yelve, N.P.; Tomar, R.; Desai, S.; Vittal, S. Active vibration control of cantilever beam by using PID based output feedback controller. *J. Vib. Control* **2012**, *18*, 366–372. [[CrossRef](#)]
- Qiu, Z.-c.; Han, J.-d.; Zhang, X.-m.; Wang, Y.-c.; Wu, Z.-w. Active vibration control of a flexible beam using a non-collocated acceleration sensor and piezoelectric patch actuator. *J. Sound Vib.* **2009**, *326*, 438–455. [[CrossRef](#)]
- Rodriguez, J.; Collet, M.; Chesne, S. Active Vibration Control on a Smart Composite Structure using Modal-Shaped Sliding Mode Control. *J. Vib. Acoust.* **2021**, *144*, 021013. [[CrossRef](#)]
- Caruso, G.; Galeani, S.; Menini, L. Active vibration control of an elastic plate using multiple piezoelectric sensors and actuators. *Simul. Model. Pract. Theory* **2003**, *11*, 403–419. [[CrossRef](#)]
- Botta, F.; Toccaceli, F. Piezoelectric plates distribution for active control of torsional vibrations. *Actuators* **2018**, *7*, 23. [[CrossRef](#)]
- Preumont, A. *Vibration Control of Active Structures*; Springer: Berlin/Heidelberg, Germany, 1997; Volume 2.
- Han, J.-H.; Lee, I. Optimal placement of piezoelectric sensors and actuators for vibration control of a composite plate using genetic algorithms. *Smart Mater. Struct.* **1999**, *8*, 257. [[CrossRef](#)]
- Kumar, S.; Chhabra, D. Optimal placement of piezoelectric actuators on plate structures for active vibration control using genetic algorithm. *Act. Passiv. Smart Struct. Integr. Syst.* **2014**, 9057, 905720.
- Moheimani, S.R.; Fleming, A.J. *Piezoelectric Transducers for Vibration Control and Damping*; Springer: London, UK, 2006.
- Meirovitch, L. *Elements of Vibration Analysis*; McGraw-Hill Inc.: New York, NY, USA, 1986.

30. Volterra, E.Z.E.C. *Dynamics of Vibrations*; Charles, E., Ed.; Merrill Books, Inc.: Columbus, OH, USA, 1965.
31. Whitney, S. *Vibrations of Cantilever Beams: Deflection, Frequency, and Research Uses*. Available online: <https://imechanica.org/files/Vibrations%20of%20Cantilever%20Beams%20.pdf> (accessed on 1 December 2021).
32. Palacios, J.L. *Design, Fabrication, and Testing of an Ultrasonic de-Icing System for Helicopter Rotor Blades*. Ph.D. Thesis, The Pennsylvania State University, University Park, PA, USA, 2008.
33. Mirjalili, S. *Evolutionary algorithms and neural networks*. In *Studies in Computational Intelligence*; Springer: Berlin/Heidelberg, Germany, 2019.
34. Holland, J.H. *Adaptation in Natural and Artificial Systems: An Introductory Analysis with Applications to Biology, Control, and Artificial Intelligence*; MIT Press: Cambridge, MA, USA, 1992.
35. Mathew, T.V. *Genetic Algorithm*; IIT Bombay: Powai, India, 2012.
36. Wang, S.-C. Genetic algorithm. In *Interdisciplinary Computing in Java Programming*; Springer: Berlin/Heidelberg, Germany, 2003; pp. 101–116.
37. PZT5A & 5H Materials Technical Data (Typical Values). Available online: http://venividiwiki.ee.virginia.edu/mediawiki/images/9/95/PZT_5Aand5H.pdf (accessed on 1 December 2021).